Neutral Meson Photoproduction from Complex Nuclei*

R. A. SCHRACK†
University of Maryland, College Park, Maryland, and National Bureau of Standards, Washington, D. C.

AND

J. E. LEISS AND S. PENNER
National Bureau of Standards, Washington, D. C.

(Received April 20, 1962)

The angular distributions of neutral mesons produced by 170-MeV bremsstrahlung on carbon, aluminum, copper, cadmium, and lead have been obtained through the coincident detection of the decay photons by a scintillation counter system. The experimental data have been analyzed by means of a Monte Carlo prediction based on an impulse-approximation elastic coherent production model. The nuclear density distributions which were used in the synthesis of those predictions which were in best agreement with the experimental data from this experiment have been compared to the charge density distributions inferred from electron scattering experiments. The values of the rms radii of nuclear matter obtained in this experiment are, within the limits of error of the experiment (about 2×10^{-14} cm), consistent with the values of charge distribution radii obtained in electron scattering.

The spin-independent part of the neutral meson photoproduction cross section used in the synthesized predictions is obtained using the dispersion theory of Chew, Low, Goldberger, and Nambu. The dependence of the cross section on the meson-nucleon phase shifts used is investigated and a set of phase shifts is presented that results in a correct prediction of the absolute cross sections observed in this experiment; however, this particular set of phase shifts is not unique.

I. INTRODUCTION

THE angular distributions of neutral mesons produced on complex nuclei N by 170-MeV bremsstrahlung by the process

$$\gamma+N\rightarrow\pi^0+N'$$

have been measured by detecting the neutral meson decay photons

$$\pi^0\rightarrow\gamma+\gamma,$$

in coincidence. The experimental results have been interpreted in terms of a simple Born approximation theory to obtain information on the nuclear matter distribution in complex nuclei. An earlier work which reported results for carbon showed the effectiveness of the technique and demonstrated good agreement with the results of electron scattering experiments.[1] Subsequent to the work reported on carbon the experimental technique was modified to obtain better angular resolution. This paper reports results for carbon, aluminum, copper, cadmium, and lead and is a more complete report of work on which a brief presentation of data and preliminary conclusions were presented earlier.[2] In obtaining the results given in this paper a more sophisticated technique of analysis has been employed. Because direct analysis of the data is extremely difficult, angular distributions were synthesized using a Monte Carlo technique based on an elastic coherent production model. The angular distributions thus synthesized for various nuclear matter distributions were then compared with the observed data.

II. THEORETICAL BACKGROUND

The "elastic coherent production" model used to synthesize results in this work has been used before in the analysis of meson photoproduction experiments.[3–7] In this model it is assumed that the major contribution to the cross section is from processes that leave the nucleus in the ground state. In the calculations presented here Born and impulse-approximation assumptions are made in the development of the matrix element for the production process.[8,9] Specifically, the assumptions made are that (1) the outgoing meson can be represented by a plane wave, (2) the total photoproduction amplitude can be represented by a superposition of amplitudes of contributions by the individual nucleons, (3) the binding forces of the nucleus can be ignored during the photoproduction process, and (4) the photoproduction operator is not dependent on the isotopic spin of the nucleon.

The differential cross section in angle for photoproduction of neutral mesons in the center-of-mass system can be written

$$d\sigma=|H|^2(k/\nu^*)d\Omega,$$

* Supported in part by the Atomic Energy Commission, Division of Research.

† Part of a dissertation submitted in partial fulfillment of the requirements for the Ph.D. degree in Physics at the University of Maryland (June 1961).

[1] J. E. Leiss and R. A. Schrack, Revs. Modern Phys. **30**, 456 (1958).

[2] R. A. Schrack, S. Penner, and J. E. Leiss, Nuovo cimento **16**, 759 (1960).

[3] E. L. Goldwasser, L. J. Koester, Jr., and F. E. Mills, Phys. Rev. **95**, 1692 (1954).

[4] A. S. Belousov, S. V. Rusakov, and E. I. Tamm, Soviet Phys.—JETP **8**, 247 (1959).

[5] G. Davidson, Ph.D. thesis, Massachusetts Institute of Technology, 1959 (unpublished).

[6] G. deSaussure and L. S. Osborne, Phys. Rev. **99**, 843 (1955).

[7] A. Odian, G. Stoppini, and T. Yamagata, Phys. Rev. **120**, 1468 (1960).

[8] G. F. Chew and G. C. Wick, Phys. Rev. **85**, 636 (1952)

[9] G F. Chew and M. L. Goldberger, Phys. Rev. **87**, 778 (1952).

where H is the matrix element for photoproduction and k and ν^* are, respectively, the meson and photon momentum in the center-of-mass system. The matrix element may be written

$$H=A\langle\psi_f|T|\psi_i\rangle,$$

where A is the number of nucleons in the nucleus, ψ_i and ψ_f are, respectively, properly antisymmetrized wavefunctions of the initial and final states of the nucleus, and T describes the photoproduction operator acting on one nucleon alone. The operator may be written as a sum $T=\mathbf{K}\cdot\boldsymbol{\sigma}+L$, where $\mathbf{K}\cdot\boldsymbol{\sigma}$ is the spin-dependent term and L is the spin-independent term.

The spin-dependent term can be expanded into three terms

$$\mathbf{K}\cdot\boldsymbol{\sigma}=K_+\sigma_+ + K_-\sigma_- + K_z\sigma_z.$$

The first two terms are spin-flip terms and the third is the non-spin-flip (NSF) term. While all nucleons can contribute coherently in spin-independent production only a few nucleons at most can contribute coherently in spin-flip production. In addition the spin-flip terms are not coherent with the spin-independent terms. The contributions from the spin-flip terms are, thus, much less important than the spin-independent term in nuclei with spin and nonexistent for elastic coherent production from zero-spin nuclei. The contribution of the spin-dependent NSF term is much less than the contribution of the spin-independent term because the production amplitudes from nucleons with paired spins will tend to cancel, and, thus, production from this term would occur mainly from the nucleons with unpaired spins. Nuclei with zero spin would, therefore, have very low (or zero) contribution from the NSF term.

Another possible experimental source of contribution to meson production at forward angles is the inverse decay process

$$\gamma+\gamma\rightarrow\pi^0$$

where one photon is the incident x-ray and the other is a virtual photon of the Coulomb field of the nucleus.[10–12] The effect has been calculated and found to have a negligible contribution in the energy region of this experiment.

From the above discussion, one can conclude that the spin-independent term will be the major contribution for all nuclei and the only large contribution for zero-spin nuclei. It is interesting to note that since the spin-flip cross section has a $\cos^2\theta^*$ angular dependence, the existence of a spin-flip contribution would be most evident in non-zero-spin nuclei for neutral meson production at $\theta^*=0°$ and 180°. (θ^* is the meson colatitude in the center-of-mass system.)

Since in the Born approximation the photon and meson are represented by plane waves, the spin-independent photoproduction operator can be redefined to show this explicitly by the expression

$$Le^{-i(\mathbf{q}\cdot\mathbf{r})},$$

where $\mathbf{q}=\boldsymbol{\nu}^*-\mathbf{k}$ is the recoil momentum of the nucleus and L is a term in the matrix element arising from angular momentum conservation, coupling constants, and other factors. The form of L is given by the fourth term of Eq. 22.5 in reference 13. All isotopic-spin-dependent terms given by Eq. 22.7 of reference 13 are also spin dependent. L is therefore the same for neutrons and protons. Experimentally determined phase shifts used in the evaluation of L are given in Sec. VI of this paper. To the extent that L is independent of nucleon variables it may be taken outside the brackets. The matrix element can now be written

$$H=AL\langle\psi_f|e^{-i(\mathbf{q}\cdot\mathbf{r})}|\psi_i\rangle.$$

For elastic coherent production the matrix element reduces to

$$H=AL\langle\rho(\mathbf{r})e^{-i(\mathbf{q}\cdot\mathbf{r})}\rangle,$$

where $\rho(r)$ is the density distribution of nucleon centers and the bracketed expression is then the Fourier transform of the nucleon density distribution and is termed the form factor, $F(q)$. One then has for the cross section from complex nuclei

$$d\sigma=A^2L^2F^2(q)(k/\nu^*)d\Omega=A^2F^2(q)\sin^2\theta^*(\mathfrak{L}^2k/\nu^*)d\Omega,$$

where in the second form of the equation $L^2=\mathfrak{L}^2\sin^2\theta^*$ has been written to show the explicit angular dependence of the cross section.

The spin-independent part of the photoproduction cross section L used in the analysis was calculated using the formalism of Chew, Goldberger, Low, and Nambu (CGLN).[13]

There are a number of shortcomings to the model used in the analysis, some more important than others. First, the extent of the contributions from inelastic production is not known. Other experiments have indicated that elastic production is still the predominant effect in protoproduction by 250-MeV x rays.[3,6]

Second, the assumptions of the impulse approximation are not all of equal validity. The outgoing meson is not well represented by a plane wave. Experimental data from charged-meson scattering experiments indicate that for free charged mesons of energies considered in this experiment the mean free path in nuclear matter is several nuclear radii.[14] Although the meson mean free path is comparable with the nuclear size and one might, therefore, expect considerable distortion of the meson wave because of the interaction with the nucleus there are several factors which may modify the amount of distortion. In the normal case of potential well scattering, the s-wave phase shifts are the most important contributors to the distortion of the wave.

[10] V. Glaser and R. A. Ferrell, Phys. Rev. **121**, 886 (1961).
[11] C. Chiuderi and G. Morpugo, Nuovo cimento **19**, 497 (1961).
[12] H. Primakoff, Phys. Rev. **81**, 899 (1951).
[13] G. F. Chew, M. L. Goldberger, F. E. Low, and Y. Nambu, Phys. Rev. **106**, 1345 (1957).
[14] F. H. Tenney and J. Tinlot, Phys. Rev. **92**, 974 (1953).

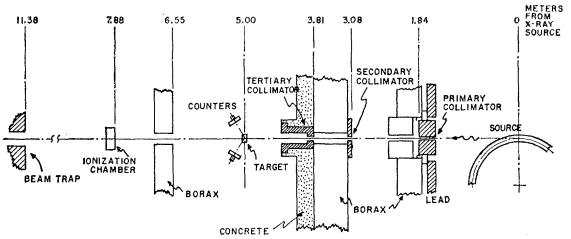

FIG. 1. Plan view of experimental layout.

A partial-wave analysis of the outgoing meson in the center-of-mass system has no s-wave component for the π^0 production from zero-spin nuclei because the incident photon has no $m_z=0$ component. Thus, a major source of distortion of the outgoing meson wave is absent. This condition is also obtained for spin-independent π^0 and for spin-dependent NSF π^0 production from all nuclei. The distortion of the p-wave component may be greater than the normal case, however, because of the strong p-wave nature of the basic meson-nucleon interaction. For example, in the analysis of charged meson scattering from complex nuclei, it has been found that

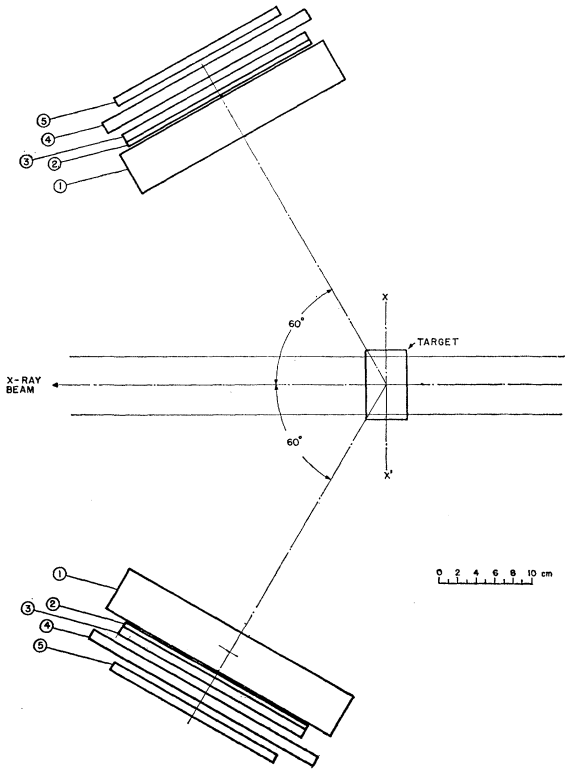

FIG. 2. Scintillation counter telescope arrangement. The counters are mounted on a yoke system that can be rotated about the axis $X-X'$ so that the angle θ_c between the counter plane and the direction of the x-ray beam may be varied. In this view, $\theta_c=0°$. Each counter telescope has the components as numbered in the diagram: (1) 5.6-g/cm² Lucite absorbers (2 in.); (2) 6.3-g/cm² lead converters ($\frac{1}{4}$ in.); (3) 9- ×9- ×$\frac{3}{8}$-in. plastic scintillator; (4) 3.4-g/cm² aluminum absorbers ($\frac{1}{2}$ in.); (5) 8- ×8- ×$\frac{3}{8}$-in. plastic scintillator.

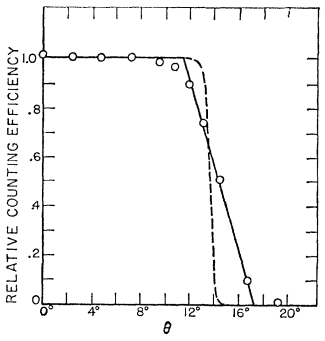

FIG. 3. Angular sensitivity of the counters. The counting rate as a function of the angle θ between the incident x-ray beam and the counter axis is shown. The dashed line indicates the angular sensitivity expected from geometrical considerations only. The points indicate the experimental measurement. Errors due to statistics are smaller than the circles shown. The solid line indicates the approximation of the angular sensitivity used in the Monte Carlo code.

the data can be fit only when the theory includes an interaction term dependent on the gradient of the nuclear matter distribution.[15,16] The gradient term arises from the strong p-wave meson-nucleon interaction. Assuming that the p-wave interaction would be evidenced in the same way for the case of the final-state interaction in neutral meson production, there would be little modification of the first falloff of the observed angular distribution which is determined in a major way by the rms radius of the nuclear matter distribution. The greatest effect of the final-state interaction should then be seen in its modification of the form factor for q values beyond the first falloff. The inclusion of a p-wave term with a gradient dependence would have a greater relative effect on the lighter nuclei where the surface-to-volume ratio is greater. It can be seen, in the light of the above discussion that, although there may be a failure of the Born approximation because of the interaction of the outgoing meson, it should be evidenced mainly for q values higher than the first falloff; thus, the values of the rms radius derived from this experiment may be quite accurate despite the final-state interaction of the meson.

III. METHOD OF THE EXPERIMENT

A. Experimental Layout

A plan view of the experimental layout is shown in Fig. 1. The NBS synchrotron was operated to produce a bremsstrahlung beam of peak energy of 170 MeV. The x rays from the synchrotron were collimated to produce a beam having a full-width angular divergence of 13 mrad. The pulse repetition rate of the synchrotron is 60 pulses per sec. During the meson data runs the yield pulse was adjusted to have a width at half-height

[15] W. F. Baker, J. Rainwater, and R. E. Williams, Phys. Rev. **112**, 1763 (1958).

[16] W. F. Baker, H. Byfield, and J. Rainwater, Phys. Rev. **112**, 1773 (1958).

of about 600 μsec and be approximately centered on the peak magnetic field. The resultant pulse had an energy spread of about 2 MeV. The calibration of the synchrotron peak energy is known to about 1% and the resetability is about $\frac{1}{2}$%. The x-ray beam had a diameter of 2.5 in. at the target. After passing through the target the beam intensity was monitored by a thick-walled aluminum ionization chamber calibrated at this laboratory. It is estimated to have an accuracy of about 2% in energy flux calibration for a bremsstrahlung beam.[17] The ionization chamber charge was collected on a calibrated capacitor and measured by a vibrating reed electrometer.

B. The Counter System

To obtain useful angular resolution in the determination of the π^0 angular distribution at low energies both of the decay photons of the neutral meson must be detected in coincidence. A drawing of the counter layout used is given in Fig. 2.

The light pulses from each scintillator were viewed by a 6199 photomultiplier whose output was shaped by a shorting-stub and limiter circuit.[18] The energy and angular sensitivity of the counter systems were determined by a beam of bremsstrahlung collimated to a diameter of 1.4 cm and hardened by filtration through 396.8 g/cm^2 of carbon. The experimentally determined angular sensitivity of a counter telescope for 90-MeV bremsstrahlung is shown by the open circles in Fig. 3. The angular sensitivity for 60- and 120-MeV bremsstrahlung was also measured and was not apparently different. The solid line indicates the approximation used in the Monte Carlo calculations. The dashed line indicates the angular sensitivity that would be expected from geometrical considerations only. The observed angular sensitivity represents an increase in counter area of 8% as well as a more diffuse counter edge. This effective increase in counter size is seen as the result of the greater probability of counting at least one member of the positron-electron pair as opposed to counting neither member of the pair generated in the lead converter near the counter edge by the incident photon.

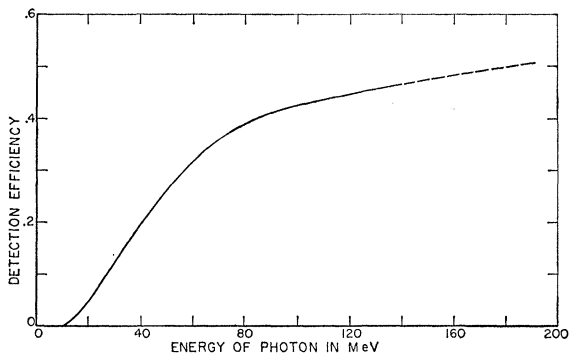

FIG. 4. Detection efficiency of the counters. The solid portion of the curve is the experimental determination of counter detection efficiency. The dashed portion of the curve is an extrapolation based on the energy dependence of the photon absorption in the lead converter.

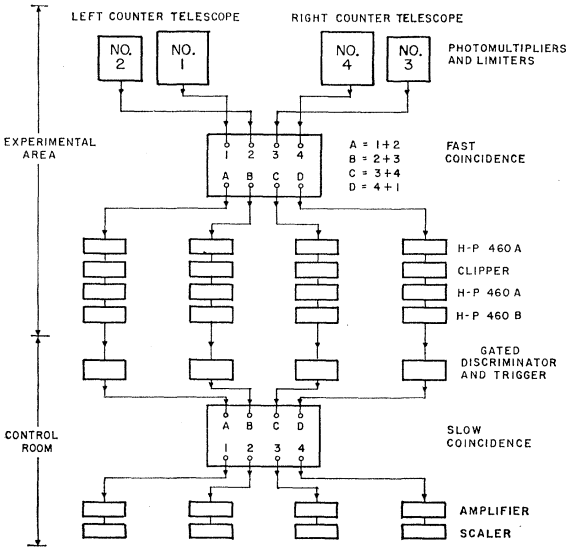

FIG. 5. Block diagram of electronics.

The energy sensitivity of the counters used in the Monte Carlo calculation is shown in Fig. 4. This curve was determined by the analysis of a counter activation curve. The range of photon energies encountered in this experiment is 34 to 135 MeV. Tests indicated that when both decay photons were detected in the geometry of this experiment the use of anticoincidence counters to insure π^0 detection only was unnecessary.

C. Targets

The targets were made in the shape of 3-in. diam disks and were suspended in the x-ray beam by a polystyrene foam holder with string supports. The thicknesses were chosen so that all targets would have about the same thickness in radiation lengths to give approximately the same background.

D. Electronics

A block diagram of the electronic equipment is shown in Fig. 5. This system was originally developed by Leiss and Robinson.[18] Two sets of coincidence circuits were used, the first of which eliminated the high background of single pulses that would otherwise jam successive circuits. This first coincidence circuit was operated with a resolution of about 8 nsec. The coincidence signals from the first coincidence circuit were used to drive gated trigger circuits which operated only during the x-ray yield. The outputs of the trigger

[17] John S. Pruitt and Steve R. Domen, Natl. Bur. Standards Monograph **48** (1962).

[18] J. E. Leiss, Ph.D. thesis, University of Illinois, 1955 unpublished).

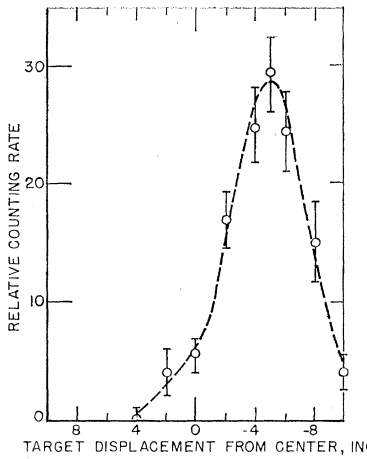

FIG. 6. Counting rate as a function of target placement. The figure shows the change in counting rate obtained when the copper target was moved along the axis of the x-ray beam. The displacement is measured with respect to the axis $X-X'$ shown in Fig. 2. The dashed curve is a smoothed curve through the experimental points.

circuits operated a slow coincidence matrix that could be programmed to register any coincidence or anticoincidence pattern desired on the output channels. This second coincidence circuit had a resolution of about 100 nsec. The background due to cosmic rays was reduced to about 8% of a nongated system.

No loss of counts due to jamming was indicated by an experimental test in which the x-ray yield rate was varied from twice to one-tenth the normal operating level with no statistically significant variation in the ratio of meson yield rate to x-ray yield rate. It is estimated that the adjustment of the coincidence circuits was such that there was a loss of not more than 2% of the true coincidence counts.

E. Experimental Procedure and Data

The data were taken at x-ray yield rates such that the accidental rate was at least an order of magnitude less than the true coincidence rate. Accidental rates were determined consecutively with the regular data runs at all angles at which data were taken.

The no-target background counting rate was determined as a function of angle. Comparison of the data with a Monte Carlo run for a column of air one meter long centered on the target position indicated that the no-target background is largely from neutral mesons produced in the air by the x-ray beam.

The counting rate for counters at 90° to the x-ray beam as a function of target position along the axis of the x-ray beam is shown for the copper target in Fig. 6. The effect of target position on observed angular distribution was less pronounced with other targets. Monte Carlo calculations for copper indicate the effect is a maximum for counter angles around 90°. An uncertainty in positioning the target of $\pm\frac{1}{8}$ in. was estimated. For copper, a target positioning error of $\frac{1}{8}$ in. could lead to a counting rate error of about 20% as well as to a change in the observed angular distribution. The error for other elements would not be as great.

TABLE I. Experimental data [10^{-36} counts/MeV (atom/cm^2)]

Counter angle (lab) (deg)	Carbon	Aluminum	Copper	Cadmium	Lead
0	13.99±1.32	75.76±8.9	161.8 ±33.3	405.2 ± 86.9	482.4±184.0
22.5	19.35±1.23	79.57±7.1	242.1 ±24.6	272.7 ±108.0	374.4±154.0
45.0	28.91±1.41	82.67±8.27	205.8 ±19.2	235.0 ± 50.6	193.3± 84.0
55.0	...	...	...	130.7 ± 33.6	67.9± 36.0
67.5	27.71±1.60	65.00±4.18	84.1 ±12.8	59.0 ± 12.3	59.2± 44.0
72.0	30.79±1.59	...	...	...	...
78.0	...	...	34 7 ± 5 9	10.1 ± 10.8	...
90.0	23.03±0.97	36.78±2.5	15.1 ± 5.7	28.2 ± 6.9	41.8± 23.0
100.0	...	...	...	...	...
102.0	...	...	10.1 ± 3.6	...	...
112.5	12.83±0.56	16.47±1.3	9.71± 4.5	18.46± 4.7	12.2± 19.0
123.0	...	...	17.0 ± 2.6	...	...
135.0	6.62±0.39	5.56±0.67	18.7 ± 2.6	14.85± 4.3	7.0± 10.4
150.3	3.81±0.46	3.02±0.52	7.97± 3.6	6.9 ± 3.6	13.9± 15.6
180.0	1.85±0.39	2.57±0.41	5.90± 2.4	2.5 ± 4.7	1.7± 12.2

The neutral meson counting rates and associated errors due to counting statistics are given as a function of angle in Table I. The counting rate is given in terms

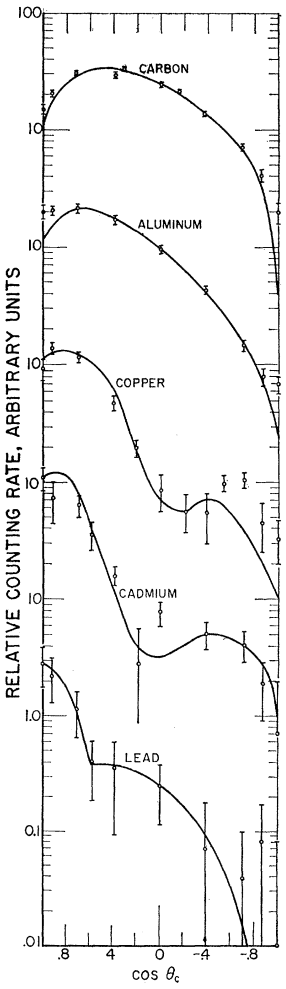

FIG. 7. Experimental data and best synthesis fits of angular distributions of decay photons of neutral mesons from carbon, aluminum, copper, cadmium, and lead. The solid curves are the lowest χ^2 fits for trapezoidal models when fit to the full angular distributions (except for carbon and aluminum, where the points near 0 and 180° were not included, as discussed in the text). The trapezoidal model parameters of the best fits are given in the first columns of Tables II and III. This figure has the same data points shown as Fig. 1 of reference 2 but the synthesized predictions shown here are obtained by a Monte Carlo synthesis code. The ordinate is logarithmic and successive curves are shifted vertically one decade for illustrative purposes.

of counts per MeV of x-ray intensity incident on the target per atom per cm^2 in the target. The intensity was calculated in terms of the same Bethe-Heitler bremsstrahlung spectrum used in the Monte Carlo code.[19] The values given have been corrected for temperature and pressure effects on the ionization chamber as well as for cosmic rays, no-target background, and accidentals. Figure 7 shows the angular distributions obtained experimentally, together with best fits (based on shape) synthesized by the Monte Carlo code.

IV. ANALYSIS

The Monte Carlo Code

Because of the continuous nature of the bremsstrahlung spectrum, and because the data were taken at only one peak bremsstrahlung energy, it was not possible to work backwards in the analysis from the observed data to an originating cross section. In lieu of a direct reduction of the data the experiment was analyzed by synthesizing an observation with a Monte Carlo code based upon the physical model presumed to exist. In the code the collimated beam of bremsstrahlung initiates a chain of events, termed a track, starting with the creation of a neutral meson in the target and eventually resulting in a count on the scalers for each successfully detected event. Included in the synthesis

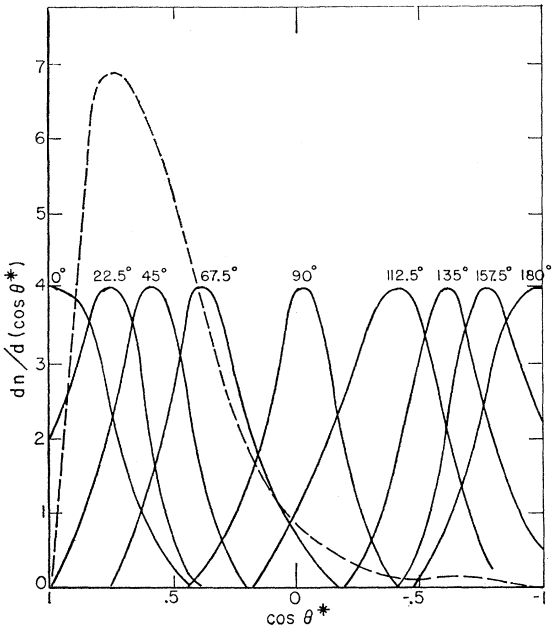

FIG. 8. Angular resolution of the counter system. The solid curves show the distribution of meson colatitudes in the center-of-mass system that are detected when the counter system plane is placed with respect to the axis of the x-ray beam at the angle (θ_c) indicated on the curve. The curves are normalized for equal height. The dashed curve indicates a typical distribution of neutral mesons that are sampled by the counters.

[19] H. Bethe and W. Heitler, Proc. Roy. Soc. (London) **A146**, 83 (1934).

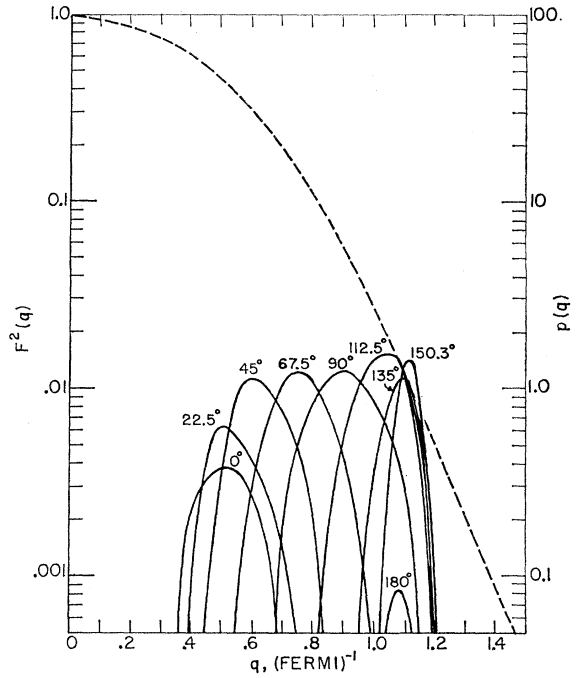

FIG. 9. Resolution of counter system in momentum transfer. The solid curves show the distribution of momentum transfers associated with meson production from aluminum. The curves are labelled by the angle, θ_c, which the counter system plane makes with the axis of the x-ray beam. The dashed curve indicates the squared form factor, i.e., the distribution in momentum transfer for the neutral mesons, assuming elastic photoproduction.

are such factors as counter efficiency in energy and angle, x-ray absorption in the target and synchrotron doughnut wall, position in the target of the photoproduction process, and the possibility of decay photon absorption in the target.

A track, once generated, was used to determine the predicted counting rate for all the counter positions used for a particular element. The colatitude distribution of scoring tracks was stored to determine the angular resolutions of the various counter positions. Figure 8 shows a set of approximate angular resolution curves in the center-of-mass system, normalized to equal height, that were obtained with the code. The angular resolution width is fairly constant in cosθ^*, which is an appropriate measure of the colatitude variable in this experiment. The shape of the angular resolution curve is dependent on all the parameters used in the code: i.e., bremsstrahlung cross section, π^0 photoproduction cross section, and counter angular and energy dependence. The bremsstrahlung cross section used was the integrated-over-angle cross section with Fermi-Thomas screening given by formula 31 by Bethe and Heitler.[19] It is interesting to note that the angular resolution curves for the counters respectively at $\theta_c=0$ and 180° cannot be centered about the counter angle. Also important is the role played by the relatively long tail on the angular resolution curves for the counter positions near 0 and 180°. The tails of the extreme-angle

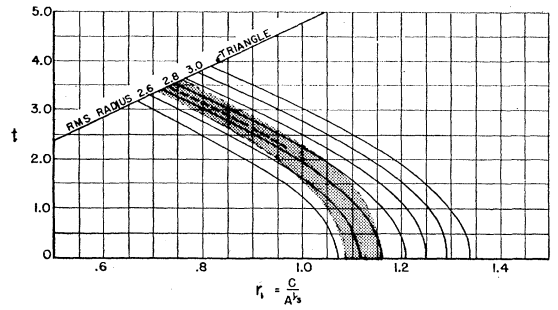

FIG. 10. Trapezoidal model fits for aluminum. The points near 0 and 180° were not included in the fitting calculations. On the dashed line χ^2 is a minimum and $\langle r^2\rangle^{1/2}=2.74\pm0.10$. The shaded area shows the region for which the χ^2 for the fit is within $\pm(2n)^{1/2}$ of the minimum χ^2, where n is the number of points included in the fitting calculation and is six for this case.

(near 0 and 180°) angular resolution curves sample angular regions having a large number of neutral mesons. Small errors in the shape of the tail caused by errors in the values of the parameters used in the code thus had a greater proportionate effect in determining the counter efficiency at extreme angle counter positions than such errors would have at counter angles near 90°. Another possible source of discrepancy between prediction of the code and experimental results at the extreme angles is based on the theoretical assumptions and is discussed in Sec. V.

In the analysis of the experimental results with the Monte Carlo calculations it became obvious that the computer time required to do a complete Monte Carlo calculation for every different nuclear matter distribution desired would be prohibitive. It was felt necessary, however, to determine the quality of fit to the experimental data of a wide range of nuclear matter distributions for every nucleus under consideration.

In order that the results of one Monte Carlo run be applied to a large number of nuclear models, the scoring probability distribution as a function of q was determined for the individual counter positions. The choice of q was weighted to correspond to a nuclear model

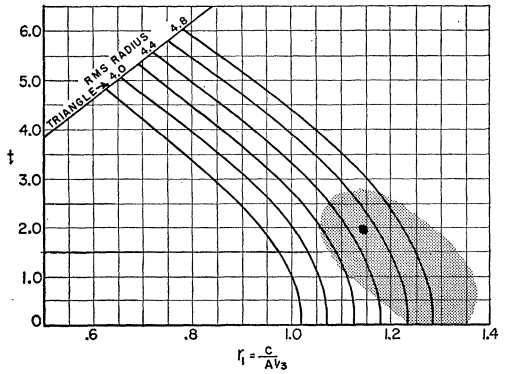

FIG. 11. Trapezoidal model fits for cadmium. All 11 data points measured for cadmium were included in the fitting calculations. The parameters at the best fit, shown by the solid circle, are $\chi^2=10.0$, $\langle r^2\rangle^{1/2}=4.53\pm0.38$, $r_1=1.15$, and $t=2.0$.

known to be a good approximation of the nucleus being examined. Results for various nuclear models were then obtained by altering the form factor which then served as a weighting function on the scoring probability distribution. The scoring probability D_{ij} for nuclear model j and counter position i was then just the weighted sum

$$D_{ij}=\sum_q p_i(q)F_j^2(q),$$

where $p_i(q)$ is the scoring probability distribution for the i counter position and $F_j^2(q)$ is the form factor squared for the j nuclear model. Figure 9 shows typical examples of the resolution of the counter system with respect to momentum transfer, $p_i(q)$.

Most of the elements were fit only with a simple trapezoidal model of nuclear density. The half-density radius (c) is given in terms of the parameter r_1:

$$c=r_1A^{1/3}.$$

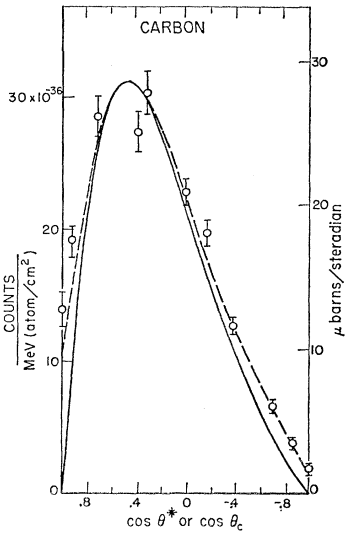

FIG. 12. Carbon experimental data and synthesis fits. In Figs. 13 through 16 the same data is presented for the appropriate elements as in Fig. 7 by the open circles. The ordinate, however, is here shown with a linear scale and the synthesis curves shown are those obtained for a unity normalization constant, $\bar{R}$. The dashed curve is the synthesis fit and the solid curve is the center-of-mass neutral meson angular distribution for photoproduction from photons of energy in the region of 165 MeV based on the parameters of the fit. The scale on the right-hand side of the graph is the ordinate for the mono-energetic photon curve and the scale on the left hand side is the ordinate of the data and synthesis curve and is the relative counting rate given in counts cm² per MeV atom. The cosθ^* abscissa is for the 165-MeV photon curve and the cosθ_c abscissa is for the data and synthesis curve. These ordinate definitions apply to Figs. 13 to 16 also.

The width of the linear falloff is given by the parameter t, which is the distance in Fermi units (10^{-13} cm) from 0.9 to 0.1 of the central density. These parameters, r_1 and t, have been widely used to describe nuclear shapes.[20] The parameters r_1 and t are varied in the fits. When $t=0$, the uniform model is obtained; when $c=t/1.6$

[20] R. Hofstadter, Revs. Modern Phys. 28, 214 (1956).

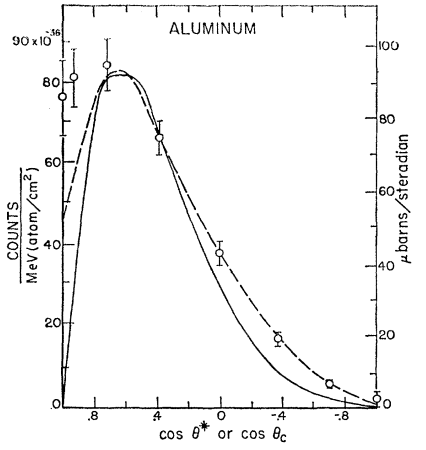

FIG. 13. Aluminum experimental data and synthesis fits. The dashed curve is the synthesis fit to the data. The solid curve is the center-of-mass angular distribution for 165-MeV photons based on the parameters of the fit.

there is no constant density portion and the triangular model is obtained. Models described by combinations of t and r_1 outside these limits are of no physical significance. For comparison purposes the carbon and aluminum data were also fit with the harmonic-well (sometimes called modified Gaussian) model.[20] No significant difference was observed between the fits obtained with the two models. Only the results for the trapezoidal model are presented.

From the values of detection probability D_{ij}, the values of the predicted counting rate C_{ij} can be computed and compared to the experimental data C_{ie} for

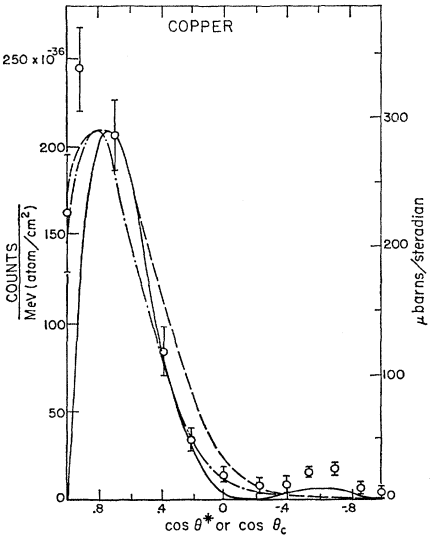

FIG. 14. Copper experimental data and synthesis fits. The dashed curve is the best synthesis fit for unity normalization and a centered target. The dot-dash curve is the synthesis obtained for the same parameters but with the target placed 0.5 cm forward of center. The solid curve is the center-of-mass angular distribution for 165-MeV photons based on the parameters of the fit.

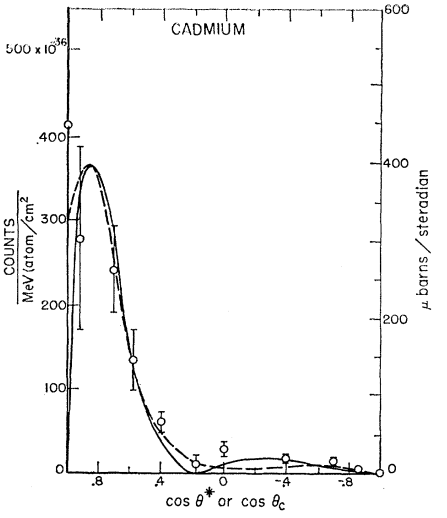

FIG. 15. Cadmium experimental data and synthesis fits. The dashed curve is the best synthesis fit to the data for unity normalization. The solid curve is the center-of-mass angular distribution for 165-MeV photons based on the parameters of the fit.

that angle. So that the normalization can be left as a variable, the ratio

$$R_{ij}=\frac{C_{ij}}{C_{ie}},$$

is calculated.

The error on R_{ij} is calculated from the errors associated with C_{ij} and C_{ie}, and the weighted mean over angles $\bar{R}_j$ is calculated. The chi-square (χ^2) of the fit of the prediction to the experimental value is calculated

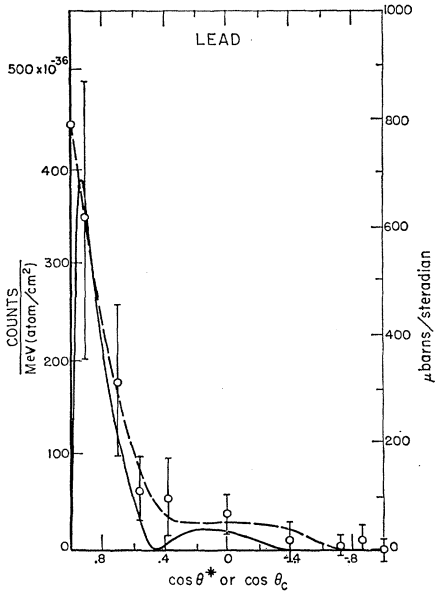

FIG. 16. Lead experimental data and synthesis fits. The dashed curve is the best synthesis fit to the data for unity normalization. The solid curve is the center-of-mass angular distribution for 165-MeV photons based on the parameters of the fit.

from the deviations of the values of R_{ij} from the mean $\bar{R}_j$ and used as a measure of the merit of the fit.

The value of χ^2 was determined in each case for a sufficiently large range of the model parameters t and r_1 to find the minimum χ^2 and the model parameter range defining one standard deviation from the minimum χ^2. For the cases of carbon and aluminum, where only the first falloff of the form factor is measured, only the rms radius (a) of the nuclear matter distribution is determined. Typical of these cases is the fitting curve for aluminum shown in Fig. 10. With elements of higher A, the form factor curve for higher values of qa is measured; thus, more information about the nuclear matter distribution may be inferred. With cadmium the second peak of the form factor is measured. As can be seen in Fig. 11, some information about the shape of the nuclear matter distribution is obtainable in that a thickness parameter t may be assigned to the best fit. The curves shown in Fig. 7 are based on the best fits, as determined by the lowest chi-square value without regard to the normalization constant $\bar{R}$, obtained from fitting curves such as Figs. 10 and 11. In the following section the best fits consistent with unity normalization are discussed and shown in Figs. 12 through 16.

V. ESTIMATES OF CROSS SECTIONS FOR MONOENERGETIC PHOTONS

Although the complicated nature of the neutral meson detection process makes a unique determination of the angular distribution of the neutral mesons difficult, it may be useful to present an estimate derived from the best synthesis fit to the data. The observed counting rate due to incident photons of a particular energy is dependent on the product of the bremsstrahlung cross section, meson production cross section, and the effective counter sensitivity. The energy dependence of these factors combine to make meson production by photons with energies in the vicinity of 165 MeV most important. The inferred differential cross section for neutral meson photoproduction for 165-MeV photons is presented in Figs. 12 through 16, together with the data and the best synthesis fit for a unity normalization constant. The ordinates are microbarns per steradian for the 165-MeV photon cross section and counts per MeV per atom per cm^2 for the data and best synthesis fit. The ordinates are scaled so that the two curves will have the same peak value on the graphs. The abscissa for the monoenergetic photon cross section is in terms of the center-of-mass colatitude of the meson, while the abscissa for the data and synthesis is the laboratory colatitude of the counters.

Several factors contribute to make the monoenergetic 165-MeV cross section prediction differ from the synthesis curve. The factors can be separated into the effects due to: (1) the fact that the photon beam is a bremsstrahlung spectrum and not monoenergetic and that as a result the cross sections of other energies contribute to the synthesis, (2) the energy and angular resolution of the counters tend to smear out the angular distribution, and (3) the center-of-mass to laboratory transformation modifies the angular distribution.

For carbon and aluminum the fit of the synthesis to the data is quite good except in the vicinity of 0 and 180°. In the case of carbon the synthesis is about 20% low in these regions. This discrepancy may be due to errors in the parameters used to define the counters. The assumed monoenergetic 165-MeV prediction is, therefore, thought to represent fairly accurately the true spin-independent part of the neutral meson cross section.

In the case of aluminum the discrepancy between the synthesis and data near 0 and 180° is much greater than for carbon. Since it does not seem reasonable to ascribe the total discrepancy to errors in the counter parameters, it is probable that the monoenergetic prediction at 165-MeV is also in error. Aluminum has a spin of 5/2 as opposed to the case of carbon, with a spin of zero. A spin-flip contribution, which has a $\cos^2\theta^*$ dependence, may be causing the observed discrepancy. It is estimated that the counter position at $\theta_c=0°$ is about a factor of 4 more sensitive to a $\cos^2\theta^*$ term than it is to a $\sin^2\theta^*$ term. This would imply a contribution of approximately 10% in cross section by a spin-flip term of form

$$\sigma(\theta^*)=(0.10)[(3/8\pi)\sigma_t(\text{S.I.})A^2F^2(q)]\cos^2\theta^*,$$

where σ_t(S.I.) is the spin-independent part of the total meson photoproduction cross section from hydrogen. A rough calculation indicates that such a term has a negligible effect on the nuclear size inferred from the data. It is also possible that transitions to the numerous low-lying excited states in aluminum are contributing to the observed cross section. Another possible source of the observed discrepancy may be the distortion of the outgoing meson wave by the meson-nucleon interaction. This effect would presumably enhance the back angles but still yield vanishing cross section at 0 and 180 deg. Because we cannot *a priori* determine which of the various suggested causes of the discrepancy should be chosen, the spin-independent monoenergetic 165-MeV angular distribution is shown without modification.

The case of copper is more complicated than that of aluminum because of two additional factors: (1) The effect of a possible experimental uncertainty in the target position on the angular distribution is greatest for copper and (2) the second maximum of the form factor begins to make its appearance in the angular distribution. Because of the possible uncertainty in target position two synthesis curves are shown, one for a properly centered target and one for a target 0.5 cm forward of the proper position. It is felt that the latter curve fits the data somewhat better, at least for the first falloff part of the angular distribution. It can be seen that the synthesis angular distributions are not high

enough in the back angles where the second maximum exists. As in the case of aluminum, this may be caused by contributions from: (1) spin-dependent effects, (2) excited-state effects, or (3) final-state interactions of the meson.

The number of low-lying excited states for copper is much greater than for aluminum. The form factor for excited state photoproduction presumably would cause the contribution to the angular distribution from excited states to be greatest in the back angles. Because of the uncertainty as to the source of the discrepancy it is not possible to modify the monoenergetic synthesis. One may estimate that the synthesized monoenergetic 165-MeV spin-independent angular distribution is low in the region of the second maximum by a factor of from 2 to 4 from the observed cross section.

The agreement of the cadmium synthesis and data is better than for copper. It may only be fortuitous that cadmium has fewer low-lying excited states. In any case, the same arguments apply as with the previous elements, but the monoenergetic 165-MeV spin-independent angular distribution is felt to be a fairly accurate representation of the cross section.

With lead, as with cadmium, the agreement between synthesis and data is fairly good and the number of low-lying excited states is not very great. Also, as with cadmium, the majority of the lead isotopes have zero spin. It is felt that within the accuracy of the data, the monoenergetic 165-MeV spin-independent angular distribution represents the true cross section fairly accurately.

Future experiments are planned to resolve some of the uncertainties in this work.

VI. DISCUSSION OF RESULTS

A. Normalization

Since the Monte Carlo code predictions are absolute, there are two types of information that can be obtained by comparison of the code predictions to the experimental results: namely, shape and magnitude. The merit of the shape fit is determined by the chi-square test, which leaves the normalization constant $\bar{R}$ as a free variable. The magnitude of the code prediction is dependent on the phase shifts used in the CGLN formalism to determine the spin-independent part of the photoproduction cross section. As has been pointed out, predictions of the photoproduction cross section in this energy region are highly dependent on the values of the small phase shifts used.[21] The variation of the spin-independent part of the cross section with phase shift has been investigated and comparisons made of the effect of using sets of phase shifts from various sources.[22] The comparisons indicated that a major variation was produced by the uncertainty in the value of the δ_{13} phase shift. With the arbitrary assumption that all other phase shifts are chosen correctly, the δ_{13} phase shift coefficient was adjusted to give unity normalization to the best fits to first falloff of the angular distributions for carbon, aluminum, and cadmium. This unity normalization producing set is

$$\delta_{11}=-0.02\eta^3,$$
$$\delta_{13}=+0.02\eta^3,$$
$$\delta_{31}=-0.04\eta^3,$$
$$\delta_{33}=[0.1066\eta^3/\omega(1.0-0.461\omega)],$$

where $\omega^2=1+\eta^2$ and η is the reduced meson momentum: $\eta=k/\mu c$, with μ the meson mass and c the speed of light. It should be noted that this is a highly interdependent set, and individual coefficients cannot be altered without destroying the validity of the set even for this experiment. This phase-shift set produces an $\bar{R}=0.60\pm0.16$ for the best fit to the first falloff for copper. This low value of the normalization constant for the case of copper may be due to an error in target placement, for when a calculation is made with the assumption of a target displaced 0.5 cm forward of the proper position, a normalization constant near unity is obtained. A low value of $\bar{R}$ is also obtained for best shape fit for lead, but the uncertainty associated with it is so great that the lack of agreement is not considered significant. Taking all experimental uncertainties into consideration, the uncertainty on the unity normalization is about 12%.

Using the phase-shift set given above, together with the s-wave phase shifts,

$$\delta_1=0.173\eta,$$
$$\delta_3=-0.110\eta,$$

reported by Puppi, one can obtain the ratio of the spin-independent part to the total neutral meson photoproduction.[23] This ratio has been applied to the experimental results for the neutral meson photoproduction from hydrogen obtained in other experiments and the modified results are shown in Fig. 17.

The triangles show the results obtained by Goldanski *et al.*[24] The open circles show the results of Luckey *et al.*[25] The squares represent the results of Koester and Mills.[26] The dashed line shows the results of Modesitt.[27]

The spin-independent part of the neutral meson cross section for hydrogen calculated using the above phase shifts in the CGLN formalism is shown as the solid curve in Fig. 17. The value 3.55 ± 0.41 μb at 176 MeV shown as a point on the curve represents the value of the spin-

[21] J. L. Uretsky, R. W. Kenney, E. A. Knapp, and V. Perez-Mendez, Phys. Rev. Letters **1**, 12 (1958).

[22] R. A. Schrack, Ph.D. thesis, University of Maryland, 1961 (unpublished).

[23] G. Puppi, *Proceedings of the 1958 Annual International Conference on High-Energy Physics at CERN* (CERN Scientific Information Service, Geneva, 1958), Vol. 39.

[24] V. I. Goldanski, B. B. Gorvorkov, and R. G. Vassilkov, Nuclear Phys. **12**, 327 (1959).

[25] P. D. Luckey, L. S. Osborne, and J. J. Russel, Phys. Rev. Letters **3**, 240 (1959).

[26] F. E. Mills, Ph.D. thesis, University of Illinois, 1955 (unpublished).

[27] G. E. Modesitt, Ph.D thesis, University of Illinois, 1958 (unpublished)

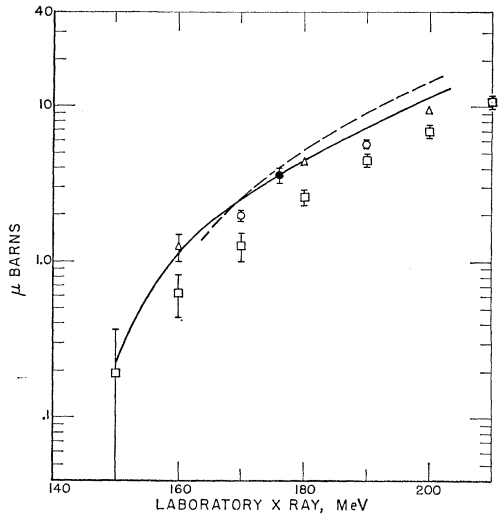

FIG. 17. Comparison of experimental results. The spin-independent parts of the total neutral meson photoproduction cross section from hydrogen as derived from various experiments are shown in comparison with the results of this experiment. The solid line is the prediction using the CGLN formalism and the unity normalization phase shifts of this report; ●, this report; △, Goldanski *et al.* (see reference 24); ○, Luckey *et al.* (see reference 25); □, Koester and Mills (see reference 26); – – –, Modesitt (see reference 27). The four sets of data from other experiments are normalized by the calculated ratio of the spin-independent part to the total meson photoproduction cross section from hydrogen (see reference 22).

independent part of the neutral meson photoproduction cross section from hydrogen as determined by this experiment and is independent of the validity of the phase shift set. The point is plotted at 176 MeV corresponding to a reduced meson momentum of $\eta=0.616$ for photoproduction from hydrogen which, in turn, corresponds to 165-MeV photoproduction from the elements reported here.

B. Nuclear Shapes

The analysis of neutral meson photoproduction yields information on the nucleon centers distribution in the nucleus. In comparing the results of this experiment with the charge shapes predicted by the analysis of electron scattering experiments it should be remembered that there are two reasons why the results should differ. The first reason is that the proton has a finite size to its charge density distribution. The charge density distribution for a nucleus can be written

$$\rho_c(r)=\int_0^\infty \rho_p(r')\rho_{pc}(r-r')d^3r',$$

where ρ_p is the charge density distribution of a proton and ρ_{pc} is the density distribution for proton centers. It, therefore, follows that the charge and proton center distributions must differ.

The second reason that results should differ is that in the meson photoproduction neutrons and protons contribute almost equally. To sum up, electron scattering experiments measure ρ_c, while neutron meson photoproduction experiments measure $\rho_{pc}+\rho_{nc}$, where ρ_{nc} is the density distribution of neutron centers.

TABLE II. Values of the rms radius of nuclear matter as determined by the fits to the experimental data. The values in the first column are determined by the best shape fit with the normalization $\bar{R}$ left as a free variable. In the second column the values are determined by the model that has unity normalization. The errors associated with the values in the second column are derived from the fractional errors in the first column.

Element	Rms radius $\bar{R}$ free	$\bar{R}=1.00$
C	2.19±0.12	2.19±0.12
Al	2.74±0.10	2.74±0.10
Cu	3.98±0.20	3.40±0.17
Cd	4.22±0.35	4.30±0.36
Pb	5.78±0.30	5.18±0.27

Because of the inability to fit with elaborate models and because of the deficiencies in the theory, it is probably not justifiable at this time to try to draw conclusions about relative neutron and proton distribution in the nucleus by comparing the results presented here with the results of electron scattering experiments.

If the value of the normalization constant $\bar{R}$ is assumed to be the same for all elements and this is taken as the deciding factor in choosing which nuclear model is correct instead of the best shape fit of synthesis to experiment, then the values of the rms radius of nuclear matter distribution obtained for copper and lead are modified. Best shape fit as well as constant $\bar{R}$ values of the rms radii are given in Table II.

In Fig. 18 the $\bar{R}=1.00$ values of the rms radii for lead and copper and the best fit (which are also the

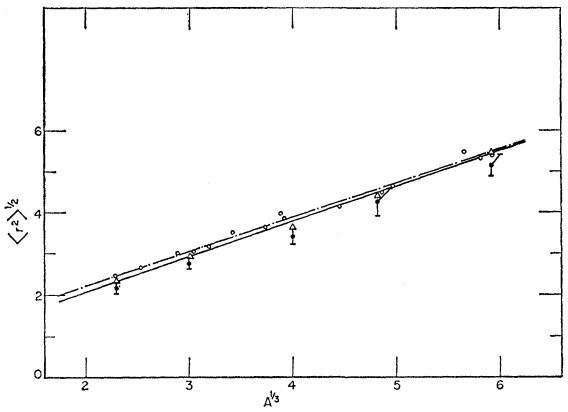

FIG. 18. Comparison of rms radii derived from electron scattering data and this work. The open circles are the values of the rms radii of charge distribution as obtained from electron scattering (see reference 20). The solid circles are the values of the rms radii of the nuclear matter distributions as obtained in this work with unity normalization. The triangles represent the values of the rms radii of the nuclear matter distributions obtained with the normalization one standard deviation below the assigned value. The dashed line is an arbitrary straight line drawn to fit the electron scattering results. The solid line is the nuclear matter distribution rms radius that would be implied by the dashed line and a proton charge distribution having an rms radius of 0.8 F.

TABLE III. Values of the r_1 and t parameters of the trapezoidal model. The values in the first column are determined by the best shape fit with the normalization R left as a free variable. In the second column the values are determined by the model that has unity normalization. The errors associated with the values in the second column are derived from the errors in the first column.

	$\bar{R}$ free		$\bar{R}=1.00$	
Element	r_1	t	r_1	t
C	$0.90_{-0.15}^{+0.35}$	$2.0_{-2.0}^{+0.7}$	$0.90_{-0.15}^{+0.35}$	$2.0_{-2.0}^{+0.7}$
Al	$0.83_{-0.15}^{+0.35}$	$3.0_{-3.0}^{+0.6}$	$0.83_{-0.15}^{+0.35}$	$3.0_{-3.0}^{+0.6}$
Cu	$1.25_{-0.05}^{+0.05}$	$0.0_{-0.0}^{+1.6}$	$1.10_{-0.04}^{+0.04}$	$0.0_{-0.0}^{+1.6}$
Cd	$1.15_{-0.10}^{+0.20}$	$2.0_{-1.2}^{+0.7}$	$1.05_{-0.09}^{+0.18}$	$2.5_{-1.5}^{+0.9}$
Pb	$1.09_{-0.15}^{+0.20}$	$4.0_{-1.5}^{+3.0}$	$1.00_{-0.14}^{+0.18}$	$3.5_{-1.3}^{+3.5}$

$\bar{R}=1.00$ fits) to the first falloff for carbon, aluminum, and cadmium are shown as filled circles. The errors associated with the values given are obtained from statistical considerations only. The open circles, through which a straight dashed line has been arbitrarily drawn, represent the rms radii of charge distribution as determined by electron scattering.[20] The solid line represents the rms radii of nucleon centers that would be inferred from the charge distribution measurements, assuming a proton charge distribution having an rms radius of 0.8 F. The triangles, which are in good agreement with the solid line derived from the charge distributions, are obtained by increasing the rms radii obtained in this experiment by about 4%, the amount corresponding to using a 12% lower normalization constant. Thus, within the ±12% uncertainty in the normalization constant the results of this experiment agree with the electron scattering data.

Table III gives the values of the parameters r_1 and t of the trapezoidal model obtained from the best fits to the full angular distributions measured in this experiment, as well as the values obtained for unity normalization. The range of error given in the cases of aluminum and carbon is determined by the triangular and uniform density models, i.e., the natural limits of the

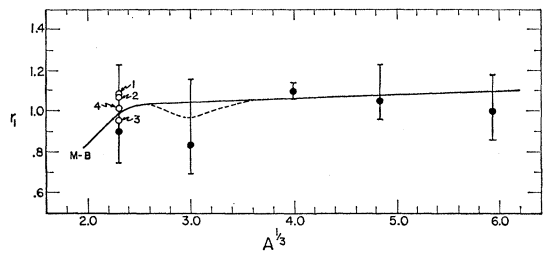

FIG. 19. Comparison of the r_1 parameter with other experiments. The unity normalization results of this experiment are shown as the filled circles. For the case of carbon, the values of r_1 as determined in other experiments are shown as open circles with the following numbers: (1) negative meson scattering by Baker *et al.* (see references 15 and 16); (2) electron scattering by Fregeau (see reference 29); (3) electron scattering by Helm (see reference 30); (4) electron scattering by Meyer-Berkhout *et al.* (see reference 28). The solid curve is from the paper by Meyer-Berkhout (see reference 28). The dashed curve is obtained when electron scattering data from magnesium, silicon, and sulphur are included (see reference 20).

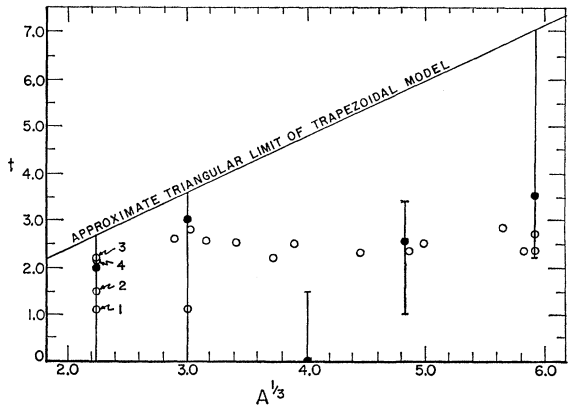

FIG. 20. Comparison of the t parameter with other experiments. The unity normalization results of this experiment are shown as the filled circles. Note that for the cases of carbon and aluminum this experiment does not define the value of t better than the natural limits of the trapezoidal model. The open circles represent the data from electron scattering; for carbon, the points are numbered and are for the same experiments as given in Fig. 19.

model, and are, therefore, not indicative of the measure of these parameters. The values for r_1 for the unity normalization case given in Table III are shown in Fig. 19, together with data obtained from electron scattering experiments. The solid line in Fig. 19 is from a graph shown in a paper by Meyer-Berkhout, Ford, and Green.[28] If electron scattering data on magnesium, silicon, and sulphur given in reference 20 are included, a dip, shown as a dashed line in Fig. 19, is indicated. Also included in Fig. 19 are some measurements of r_1 obtained from electron scattering experiments for carbon given by Fregeau[29] and Helm[30] as well as results obtained in negative meson scattering experiments given by Baker *et al.*[15,16]

Figure 20 shows the values of t obtained for the unity normalization case for the various elements in Table III.

VII. CONCLUSIONS

The angular distributions of neutral mesons obtained from complex nuclei in this experiment are in agreement in shape and in absolute magnitude with predictions based on the elastic coherent photoproduction model and meson-nucleon phase shifts in general agreement with other sources.

The results of this experiment indicate that a major portion of the observed neutral meson photoproduction cross section from complex nuclei can be explained using a simple Born approximation treatment of the elastic coherent model employing the spin-independent part of the neutral meson cross section from free nucleons. Further study is needed on the effects of the final-state interaction as well as the contribution of spin-dependent and excited-state production.

[28] U. Meyer-Berkhout, K. W. Ford, and A. E. S. Green, Ann. Phys. (New York) **8**, 119 (1959).
[29] J. H. Fregeau, Phys. Rev. **104**, 225 (1956).
[30] R. H. Helm, Phys. Rev. **104**, 1466 (1956).